Ecological Modelling 419 (2020) 108964

Contents lists available at ScienceDirect

Ecological Modelling

journal homepage: www.elsevier.com/locate/ecolmodel

Topological acoustic sensing of spatial patterns of trees in a model forest landscape

Trevor D. Lata[a,*], Pierre A. Deymier[a], Keith Runge[a], François-Michel Le Tourneau[b], Régis Ferrière[b,c,d], Falk Huettmann[e]

[a] Department of Materials Science and Engineering, University of Arizona, Tucson AZ 85721, USA
[b] Unité Mixte Internationale iGLOBES, CNRS, Ecole Normale Supérieure, Université PSL, Université of Arizona, Marshall Building, 845 N Park Avenue, Tucson AZ 85721, USA
[c] Institut De Biologie de l'ENS, Ecole Normale Supérieure, Université PSL, CNRS, INSERM, 46 rue d'Ulm, 75005 Paris, France
[d] Department of Ecology and Evolutionary Biology, University of Arizona, Tucson, AZ 85721, USA
[e] -EWHALE lab- Institute of Arctic Biology, Biology & Wildlife Department, University of Alaska Fairbanks, Fairbanks, AK 99775, USA

ARTICLE INFO

Keywords:
Acoustic
Seismic waves
Sensing
Geometric phase
Landscape
Density

ABSTRACT

Remote sensing of forest environments through sound holds promise for a renewed and extended effort in monitoring vegetation distribution and associated characteristics. Here we introduce a new acoustic sensing approach that exploits the geometric phase of ground-supported acoustic waves, such as seismic waves, resulting from their scattering by trees in forest environments. Using a simulated model forest with different spatial arrangements of trees as a testbed, we numerically calculate the geometric phase of acoustic waves and show that it is exquisitely sensitive to the spatial pattern of trees. This topological acoustic sensing modality provides a novel, quantitative, insightful way to characterize global properties of tree spatial distribution, which is fundamental to forest management. Sound has virtually never been used to support quantitative forest monitoring, and here we elaborate on the wider implications and applications of topological acoustic sensing in remote landscapes as a very promising concept.

1. Introduction

In natural forests, trees are not uniformly distributed but instead form spatially heterogeneous patterns and distinct clusters shaped by endogeneous and exogeneous processes such as fires (Larson and Churchill, 2012) or resource distribution. Larson and Churchill (2012) for instance describe tree spatial patterning in terms of clumps, individuals, and openings. A clump is a group of trees of similar size clustered together; individuals are well separated trees forming 'random' patterns; and openings are gaps in the forest that are not occupied by trees. The spatial distribution of trees in forests influences many metrics as well as dynamic processes such as timber volume, future fires, nutrient distributions and forest regeneration. Given the importance of spatial distribution, there is a need for quantitative descriptions for classifying distributions of ecological elements (Greig-Smith, 1952, 1983). While forests are not well monitored, specifically for inaccessible locations, detection of tree spatial patterns in real-world landscapes is an important component of forest monitoring, needed to inform forecasts and scenarios for sustainable forest management (Carrer et al., 2018).

Natural and human activities combine to produce sound that propagate through forests (Mullet et al., 2016). Sound can reveal dimensions and structures of landscapes that are otherwise easily overlooked, and not accessible, measured, or considered in conventional studies (Sharma, 2018; Sahin and Ince, 2009; Turner et al., 2018). Acoustic sensing and soundscape analysis yield novel insights with promising applications. Acoustic sensing provides indicators of forest structural changes, which inform about the intensity, direction, and modalities of these changes. Acoustic sounding systems can provide data about forest environmental change, and measures of the intensity of human activities and their impact (Sharma, 2018; Turner et al., 2018). Acoustic sensing can also be used to detect early warnings of forest fires (Sahin and Ince, 2009).

Conventionally, soundscape data have been analyzed in the frequency domain, using the power spectral density as a central concept (Turner et al., 2018). Such analyses, however, do not provide direct information on the nature and dynamics of heterogeneity in the spatial distribution of trees. In recent years though, topological acoustics has

* Corresponding author.
E-mail address: tlata157@email.arizona.edu (T.D. Lata).

https://doi.org/10.1016/j.ecolmodel.2020.108964
Received 16 August 2019; Received in revised form 23 January 2020; Accepted 24 January 2020

become a powerful approach to describe sound waves that now includes geometrical attributes as an additional source of information for the analysis and applications of sound waves (Deymier and Runge, 2017; Zhang et al., 2018). Topological acoustics exploits the complete range of acoustic wave properties—to extend beyond the traditional, canonical attributes of sound wave frequency (ω) and wave vector (k), and now embrace the geometric domains of amplitude (A) and phase (η). Topological acoustics exploits the geometrical characteristics of sound amplitude and phase imparted by the symmetry breaking that results when an environment, such as a forest, scatters an acoustic wave. As a result, the geometrical phase of the sound is a sensitive measure of sound-environment interactions. The power of topological acoustic sensing resides in this geometric phase being a global metric of the sound-scattering environment. Thus, topological acoustics paves the way for novel analytical strategies that extend acoustic sensing and provide a more complete sound-based characterization of forest structure. This sound-based method would allow for continuous regular monitoring over long periods of time and may help address issues of transferability associated with expensive traditional remote sensing platforms such as satellite imaging (Díaz-Delgado et al., 2017). Additionally, due to its topological nature this method may aid in developing grid-based atlases of vegetal density for a variety of grid sizes (Franklin, 2010).

Long-wavelength ground supported acoustic waves such as seismic waves (Stein and Wysession, 2009) are pertinent probes for applications of topological acoustic to sensing forest environments. This has been shown recently by the strong interaction that occurs between seismic waves of a few tens of Hz and trees from a forest (Colombi et al., 2016; Maurel et al., 2018). Here, we investigate whether and how ground supported long-wavelength acoustic waves such as seismic waves, that can propagate over great distances at the interface between ground and above-ground forest cover, provide us with information about the tree spatial pattern. Based on our previous work (Deymier and Runge, 2017) we introduce a new approach for acoustic sensing that utilizes the geometric phase of scattered ground supported acoustic waves as a highly sensitive measure of the global properties of forest spatial patterns. Thus providing a useful tool for, for instance, forest inventories on a landscape scale. In the following section, we introduce a numerical model that can be used to calculate the geometric phase of acoustic waves resulting from the scattering of ground supported waves by a model forest with different spatial tree distributions. The numerical model is based on the Green's function formalism of acoustic waves and implemented utilizing the MATLAB computing environment. In section 3, we consider a gradient of model forest structure, from a random spatial distribution of individual trees to a single clump of trees. The geometric phase of ground supported acoustic waves is shown to be very sensitive to the spatial distribution of the trees, demonstrating that topological acoustic sensing can provide a global sensing modality of forest spatial patterns. Conclusions from these results are drawn in Section 4.

2. Material and methods

2.1. Method

Conventional acoustic sensing provides spatial, temporal, and spectral data on an environment's sound field. Phase information, and more specifically the geometric phase (η), has traditionally remained outside of conventional sensing methodology. Instead, here we introduce a new approach for acoustic sensing that actually utilizes the geometric phase of scattered acoustic waves as a measure of the global properties of the scattering environment. We establish the important relation between an acoustic wave's η and its Green's function (Deymier and Runge, 2017) (see Appendix A). The acoustic Green's function represents the acoustic field supported by some environment, resulting from a "tap-like" mechanical stimulus applied at some location within this environment. For a given environment, the Green's function depends on 1) a position variable describing the field; 2) a position variable describing the location of the stimulus; and 3) the eigenvalue, which is effectively the square of the frequency of the acoustic wave, $E = \omega^2$.

The Green's function is a complex function. We first consider a normalized Green's function $\hat{G} = \frac{G}{\sqrt{G^*G}}$ where G^* is the complex conjugate of G. We have $\hat{G}(E) \propto e^{-i\eta(E)}$. We calculate the derivative of this normalized function with respect to the eigenvalue E:

$$\frac{d\hat{G}(E)}{dE} = \frac{1}{\sqrt{G^*G}}\frac{dG}{dE} - \frac{G}{2(G^*G)^{3/2}}\frac{d(G^*G)}{dE} \tag{1}$$

From this derivative, we can obtain the Berry connection (BC) (Berry, 1984) in the space of eigenvalues. BC is defined as the following quantity:

$$BC(E) = -i\,Tr\left(\hat{G}^*(E)\frac{d\hat{G}(E)}{dE}\right) \tag{2}$$

where Tr is the trace over the spatial domain spanned by the Green's function. Tr sums the quantity in parenthesis of Eq. (2) over the entire spatial domain. The Berry connection relates to a change in the η of the acoustic wave field as a whole—a global measure of the environment supporting the acoustic field. The function $BC(E)$ can then be understood to describe the variation of the η of the Green's function along a path in the space of eigenvalues, i.e., on the space of frequencies.

Using well-established Green's functions identities related to the properties of the Green's function in the space of its eigenvalues (see Appendix A for details), it is possible to show that:

$$BC(E) = \frac{d\eta(E)}{dE} = -Im(TrG) \tag{3}$$

Eq. (3) relates η to a scattering problem, i.e., the scattering of acoustic waves by the environment. The η, as a function of frequency, is an experimentally measurable quantity, which is the phase accumulated by an acoustic wave due to scattering by the environment. Topographical and structural features of the scattering environment, such as the spatial distribution of trees in a forest, are reflected in the Green's function; the value of the geometric phase is not sensitive to details or local features of the tree arrangement but is a more global measure. We can utilize the geometric phase to classify the environment in terms of global characteristics, relative for example to the spatial distribution of constitutive elements such as trees. This approach is introduced in more details below.

2.2. Model

We develop an elastic model of a forest including ground and tree cover that can be used to calculate numerically the acoustic Green's function for given tree distributions and the corresponding phase η. The method is detailed in Appendix B. This model forest is used to numerically investigate the correlation between tree distribution and η.

We model the forest landscape as a semi-infinite elastic medium (ground) supporting trees distributed in various patterns. In essence, each ground-anchored tree acts as an elastic resonator (here four resonances), which scatters ground-propagating acoustic waves. For this each tree is discretized into a one dimensional (1D) linear chain of four masses connected by elastic springs (Fig. 1(a)). The spacing between masses is denoted by a. All trees have the same height and constitution, i.e., the same characteristic vibrational resonances.

The ground is discretized into a three-dimensional simple cubic lattice of masses connected via elastic springs (Fig. 1(a)). The discrete cubic lattice is cleaved along the (001) plane (i.e. a plane perpendicular to the vertical axis) to create the surface of the ground. The masses in the cubic lattice are all identical and connected via harmonic springs along the edges of the cubic lattice. The spacing of masses in the cubic

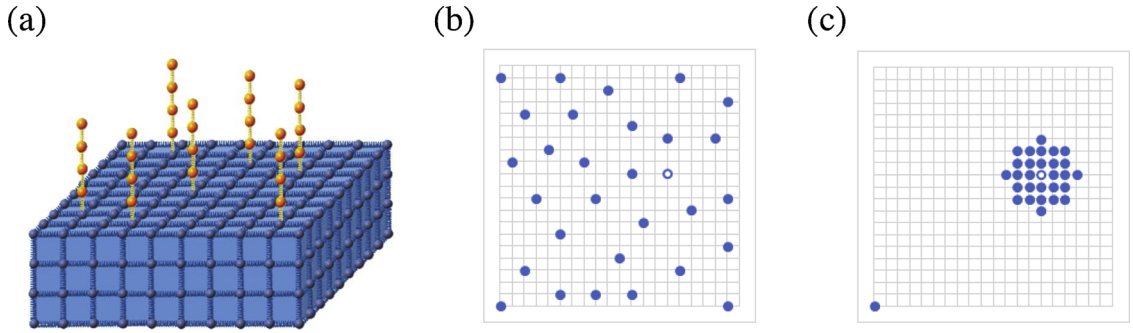

Fig. 1. (a) Model of resonating "trees" (orange) represented as one-dimensional mass-spring chains anchored elastically to the three-dimensional "ground" (blue) modeled as a simple cubic lattice of masses and springs. (b) Top view of the distribution of $N_c = 30$trees anchored to the ground surface in a $20a$ by $20a$ area in a sparse (individual) configuration used as a reference point in the model. (c) Configuration of trees in a single clump of 29 trees with the central tree (open circle) also shown in (b) for reference to the random tree configurat ion. The space spanned by the position of the trees, represented as dots, is denoted R in the text (For interpretation of the references to colour in this figure legend, the reader is referred to the web version of this article).

lattice is also equal to a. The trees are elastically anchored to the surface of the semi-infinite lattice through another elastic spring. For the sake of mathematical and numerical ease we assume that the masses and spring stiffnesses of the trees and tree anchor are identical to those of the ground. There is therefore no irregular spatial variability in the ground density or composition.

For the sake of tractability, the dynamic equations of the elastic system composed of discrete trees distributed on the discrete elastic ground are limited to displacements of masses in one single direction. The direction of the displacement is unspecified and could be representing either transverse/shear or longitudinal/pressure polarization of the sound wave. The Interface Response Theory (IRT) (Dobrzynski, 1988, 1987) enables us to calculate the elastic Green's function (more specifically the diffusion matrix) of the composite elastic medium composed of trees anchored on the ground surface. The diffusion matrix is then used to calculate the phase of the scattered wave as a function of the frequency. The method of calculation of the Green's function/diffusion matrix and the phase η is detailed in Appendix B and in Deymier and Runge (2018). Once the spectral dependency of the geometric phase, $\eta(\omega)$, is determined for a given environment, we aim at evaluating how the phase varies as the spatial structure of the environment changes. For instance, let us focus on a forest system composed of N_c mass-spring chain-like trees with a spatial distribution described by the $2N_c$ dimensional vector M on the discrete cleaved surface of the cubic lattice (i.e. ground). This vector contains the 2D coordinates of every tree. This vector spans the subspace R of M, the space of the possible locations of tree anchors, for the system defined in the Appendix B as (see Eq. (B13)):

$$R = \{p_1 = (0,0,0),\ p_2 = (x'_1, x'_2, 0),\ p_3 = (x''_1, x''_2, 0), \ldots, p_{Nc} = (x_1^{(Nc-1)}, x_2^{(Nc-1)}, 0)\}$$

where defines a 2D position on the (001) surface of the cubic lattice. The $x_l^{(i)}$ are integer multiples of the grid spacing of the cubic lattice, "a." Following Appendix B, the phase difference (normalized to π) between acoustic waves supported by the coupled system (trees elastically anchored to the ground) and by the uncoupled system (trees not anchored) is then obtained from the relation: $\eta(R\varepsilon M, \omega) = -\frac{1}{\pi} Im[\ln(det\vec{\Delta}(MM))]$ where $\vec{\Delta}(MM)$ is the diffusion matrix. The diffusion matrix relates the Green's function of the coupled system, $\vec{g}(MM)$, to that of the uncoupled system, $\vec{G}(MM)$, via $\vec{g}(MM)\vec{\Delta}(MM) = \vec{G}(MM)$ in the space M. It is then clear that since $\ln(det\vec{\Delta}(MM)) = -\ln(det\vec{g}(MM)) + \ln(det\vec{G}(MM))$, $\eta(R\varepsilon M, \omega)$ stands for the phase difference between the coupled and uncoupled system. We can now consider two possible spatial patterns of trees, namely R and R'. The quantity $\Delta\eta = \eta(R, \omega) - \eta(R', \omega)$ represents the difference between the geometric phase of pattern R and R'. The phase associated with the uncoupled system is independent of the spatial arrangement of the uncoupled mass-spring chains and therefore cancels out in the expression of $\Delta\eta$. One can consequently calculate the change in geometric phase along chosen paths in the space of all tree spatial patterns.

Here, we consider a path that takes the forest landscape from a random—but uniform— distribution of trees (Fig. 1(b)) to a clustered spatial distribution of trees (Fig. 1(c)). The forest spatial pattern evolves from individuals to a single clump. We fix the total number of trees to $N_c = 30$, located on a $20a \times 20a$ area of the ground surface. A tree was randomly selected from the starting pattern of individual trees as the center of the clump. Trees are subsequently removed randomly from elsewhere in the model among the remaining individuals, forming gaps. The selected trees are added to the clump to maintain the total number of trees constant. To limit the space of possible configurations of trees in a clump, trees were added in an anticlockwise manner, beginning from the top of the central tree. The final cluster contains 29 trees, therefore there are 29 steps in the development of the clump. This process is illustrated in Fig. 2.

3. Results

In Fig. 3 we report the calculated variation in density of states, $\Delta n(\omega)$, of the randomly distributed pattern of individual trees as a function of reduced frequency. The frequency is reduced by the dimensional multiplicative factor, $\frac{\beta}{m}$, where β is the stiffness of the springs and m is the mass of the elements in our discrete ground/forest

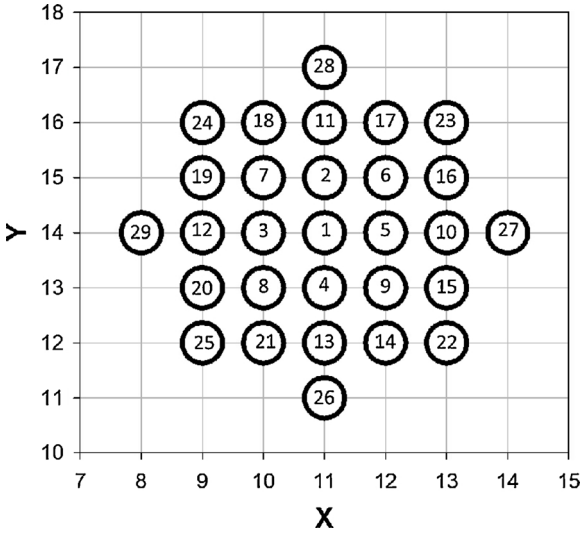

Fig. 2. Order in which trees are added to form the clump of 29 trees, with one denoting the central tree. We arbitrarily chose to add trees in an anticlockwise manner.

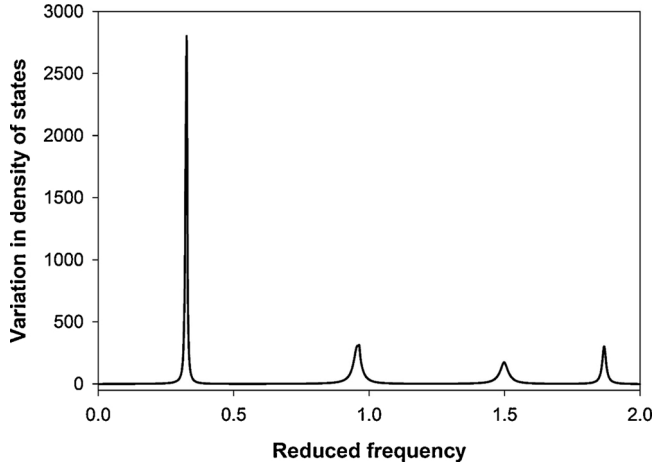

Fig. 3. Variation in density of states, Δn, of the forest pattern composed of 30 randomly distributed trees as a function of reduced frequency. The four peaks correspond to the four resonant frequencies of the mass/spring tree model. See Section 3.2 and Appendix B for model description and parameters.

model. The reduced frequency spans the interval (0, 2). This figure shows the four resonances associated with the four mass/spring model of the trees. Since the trees are separated by distances which prevent them from interacting through the elastic ground, the resonance frequencies are degenerate.

We calculate the phase η numerically as a function of reduced frequency between 0.2 and 0.4—about the first resonance of the trees. Since the phase can only be determined to within multiple of 2π, the plot of η versus frequency of Fig. 4 has been corrected for these inconsequential 2π jumps. The numerically calculated values of η were parsed through and multiples of 2π were added manually, resulting in a continuous function of η as a function of reduced frequency. The corrected phase accumulates π each time the wave encounters a resonance (i.e. the wave is scattered by a tree). Since they are 30 degenerate tree resonances at the reduced frequency of 0.327, the total accumulated phase approaches the value of 30 π.

A similar calculation of the corrected phase $\eta(\omega)$ was done for each stage of the formation of the clump of 29 trees. The initial distribution of randomly distributed individuals is used as a reference for each clump of trees. The corrected η for the configuration of individuals is

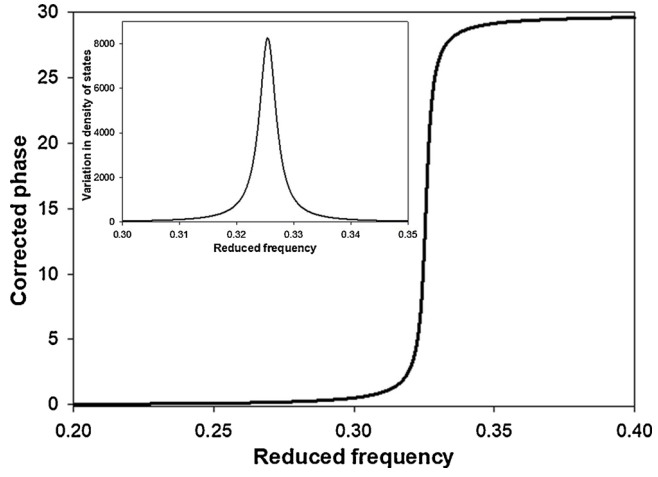

Fig. 4. Calculated phase η as a function of reduced frequency in the vicinity of the first tree resonance for the forest pattern composed of 30 randomly distributed trees. The phase is expressed in units of π. The first tree resonant frequency is approximately 0.327. Inset: Variation in density of states, Δn, corresponding to the same spatial pattern as a function of reduced frequency. See Section 3.2 and Appendix B for model description and parameters values.

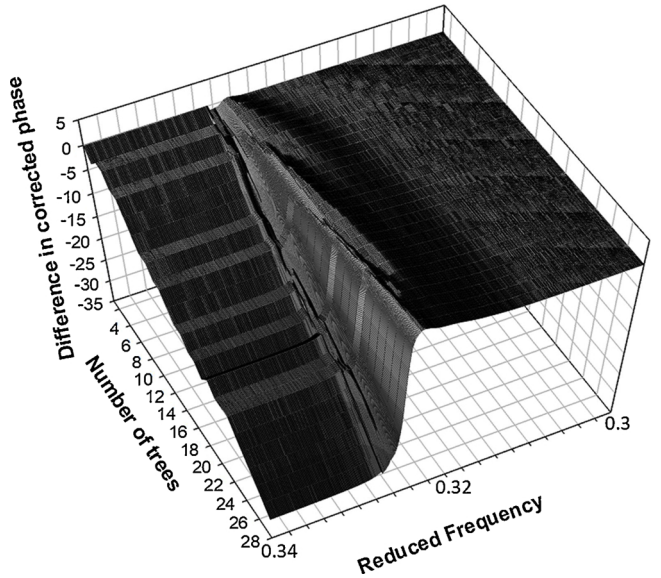

Fig. 5. Difference in corrected phase for all 29 stages of development of the clumped forest from the individual tree configuration. The axis "Number of trees" refers to the number of the trees in the clump. The difference in corrected phase refers to the phase of the forest pattern with a clump relative to that of the randomly distributed forest. The phase is expressed in units of π. See Section 3.2 and Appendix B for model description and parameter values.

subtracted from the corrected η for each stage of the clump. The resulting function is a difference in corrected phase, $\Delta\eta(\omega)$, for each clump size. In Fig. 5, we clearly see the delineation by the resonant frequency. Away and below resonance, the difference on corrected phases only weakly increases with the number of trees in the clump. Away and above resonance, the difference in corrected phase decreases monotonously as a function of clump size, approaching the value of -30 π as we remove individual trees from the forest to form the clump. The most remarkable effect resides in the vicinity of the resonant frequency where significant structure in the phase difference can be observed.

To reveal these effects more clearly, Fig. 6 shows the difference in corrected phase as a function of the number of trees in the clump at four frequencies. More specifically, we consider the two frequencies, 0.3 and 0.323 below resonance and the two frequencies, 0.3344 and 0.35 above resonance. We note the slow but monotonous increase in phase difference for the lowest frequency. Above resonance, the difference in phase appears to decrease by steps.

Slightly below resonance, the phase difference shows highly nonlinear behavior. For some ranges of clump size, the difference in phase decreases monotonously. However, these ranges are separated by discontinuities. These discontinuities are not multiples of 2π; they take on values that are fractions of π. They occur between 7-8-9 trees as well as 14–15, 18–19, and 22–23 trees in the cluster. In Fig. 7 we report the change in difference in corrected phase between clusters of increasing size. As discussed before, this difference is effectively the geometric phase.

To shed more light on the cause of the discontinuities in the difference in corrected phase (or the change in geometric phase), we focus on the jump occurring for a clump of 19 trees. The tree distribution for this clump results from adding trees 14 through 19 to a cluster of 13 trees (see Fig. 2). These trees are located in an octogonal shell $\sqrt{5}a$ away from the center of the cluster. That shell can accommodate up to 8 trees. Therefore, for the clump of 19 trees, there are two gaps (i.e. sites not occupied by trees) in that shell. We analyse the clump of 19 trees by fixing one of the gaps (the one that would eventually accommodate tree 20) and rotating the other gap (the site that would accommodate tree 21) counter-clockwise about the center of the clump. This process is illustrated in Fig. 8.

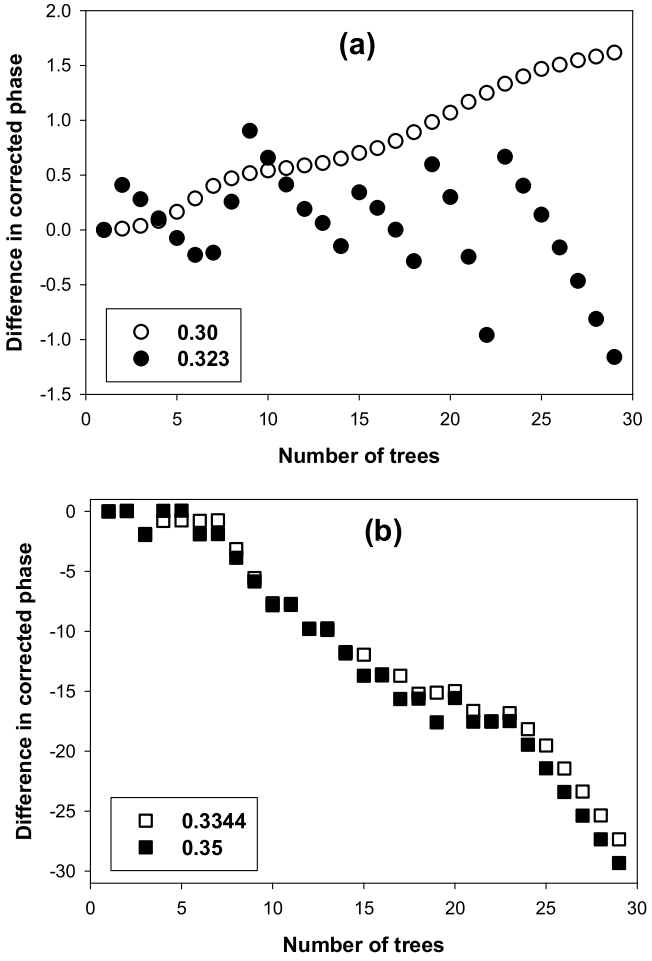

Fig. 6. (a) Difference in corrected phase at a frequency of 0.3 (open circles) and 0.323 (closed circles) as a function of the number of trees in the clump. (b) Same as (a) but for the frequencies 0.334 (open squares) and 0.35 (closed squares). The phase difference is expressed in units of π. See Section 3.2 and Appendix B for model description and parameter values.

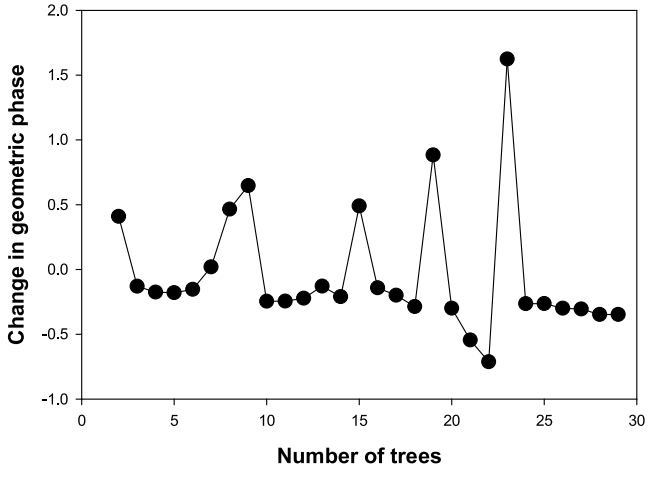

Fig. 7. Difference in the geometric phase at a frequency of 0.323 between two subsequent tree patterns as the number of trees in the clump is varied according to the prescription illustrated in Fig. 2. The geometric phase difference is expressed in units of π. See Section 3.2 and Appendix B for model description and parameter values.

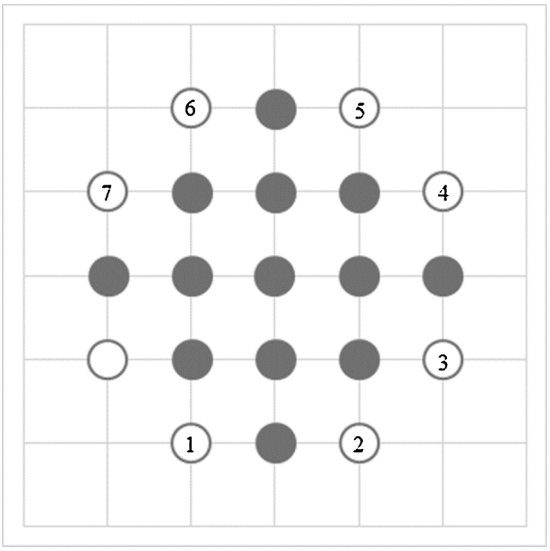

Fig. 8. Possible configurations of a clump containing 19 trees. The open circles indicate the tree sites located on an octagonal shell at a distance of $\sqrt{5}a$ from the center of the clump. The grey circles mark the position of the 13 fixed trees in the clump. The open circle represents the fixed gap (site without a tree) in the clump of 19 trees. The numbered circles show the possible location of the second gap. See text for details.

Table 1
Calculated values of the difference in corrected phase for the 7 possible configurations of trees in a $N_c = 19$ clump. See Fig. 8 for explanation related to the position of second gap in the clump.

Position of the second gap in the $N_c = 19$ clump	Difference in corrected phase (units of π)
1	0.598
3	0.605
4	0.614
5	0.584
7	0.612
2	−0.543
6	−0.543

At the reduced frequency of 0.323, the discontinuity in difference of corrected phase remains. However, the symmetry of the clump affects the value in the difference in corrected phase. In Table 1, we classify the $N_c = 19$ clumps into two classes depending on the value of the difference in corrected phase. The difference in corrected phase takes on values of approximately 0.6π for configurations 1, 3, 4, 5, 7 and approximately -0.54π for configurations 2 and 6. The two gaps in configurations 1, 2, 5 and 7 are related by mirror symmetry perpendicular to faces of the octagonal shell. Hence, they belong to the same class. The gaps in configurations 2, 4 and 6 are related by mirror symmetry passing through vertices of the octagonal shell. However, the separation distance between the gaps in configuration 4 exceeds the cut-off distance for the Green's function of $\sqrt{5}a$. Configurations 2 and 6 have gaps separated by a distance shorter or equal to the cut-off distance. These two configurations belong to the same class. These observations indicate that while the relation between phase difference and tree distribution may be quite complex, the difference in corrected phase (and/or the corresponding geometric phase) is not only a signature of the number of trees in a clump but also of the symmetry characteristics of a specific clump.

4. Conclusions

Understanding how environmental conditions shape vegetation distributions is crucial for predicting ecosystem responses to global change. Here, we have introduced an acoustic-based sensing method that may provide unique signatures of tree spatial patterning in forests. This method relies on the scattering of long-wavelength ground supported acoustic waves, such as seismic waves, by trees. Using an elastic model of a ground covered by trees, we demonstrate numerically that the phase of ground supported acoustic waves resulting from scattering by trees can provide information about their spatial distribution. We show that the scattered phase (or equivalently the geometric phase) of acoustic waves may provide a highly sensitive measure of the global properties of the tree spatial patterns. For instance, the scattered phase can be used to quantify the global change in the distribution of trees from randomly spread individual trees to a forest composed of tree clumps and gaps. It can provide crucial but lacking rapid assessment. Further, it can also be used as a quantitative measure of tree density and abundance. In addition, in the case of a forest composed of clumps, we have shown that the geometric phase is significantly affected by the symmetry of tree clumps. The model presented here was limited to trees with identical geometrical (height) and elastic properties. Trees of varying height would result in the appearance of resonant frequencies associated with each height; if these frequencies are sufficiently far apart from each other, they will not affect the change in geometric phase associated with one another. We expect that the resonant frequency may be chosen to distinguish spatial patterns in the distribution of trees of different size, age or species. This is specifically the case when using advanced methods of data mining and machine learning that can extract signals from noisy data. Additionally, the model lacks the variation in mechanical properties of the ground that would arise from differing mineral, water, and biomass content. Variations in ground composition and varying tree heights is the subject of future work. Even though the example presented here focused on a single scale, we also expect the detection of spatial patterns at different scales to be possible through the topological acoustic sensing approach.

From a practical point of view, when probing real landscapes, two approaches may be used for the implementation of a topological acoustic sensing experiment used to monitor the changes of a forest overtime. The first approach is “active” and relies on the conventional direct pulse/echo method. It requires the use of a source of ground supported waves. A single seismic detector can then be used to relate changes of the geometric phase of the emitted seismic wave to changes in the structure of the above-ground environment. A second “passive” approach relies on retrieving the Green’s function of the ground/forest scattering medium from cross correlations of the acoustic fields received by two passive seismic sensors (Derode et al., 2003; Sanchez-Sesma and Campillo, 2006; Campillo, 2006). The Green’s function between two sensors, and more specifically its phase, is reconstructed by averaging the cross correlation of waves produced by ambient seismic noise.

The topological acoustic sensing method we introduced here may be able to serve as a new modality for detecting variations in spatial patterns of trees in forest subjected to global changes over time. By adding a new dimension and metrics of topological sound, this new and innovative tool may be useful in meeting the needs for inventorying and assessing the state and evolution of remote and vast forestry landscapes as well as generating the data necessary for modeling and developing forest management strategies in a cost-effective fashion (Young et al., 2018; Ohse et al., 2009).

Funding

This research did not receive any specific grant from funding agencies in the public, commercial, or not-for-profit sectors.

Appendix A

The function $BC(E)$ given by Eq. (2), in the main text, can be understood as describing the variation of the geometrical phase of the Green’s function along a path in the space of eigen values, E, i.e., on the space of frequencies since $E = \omega^2$. Indeed, consider the two eigen values E and $E + dE$. The normalized Green’s function at $E + dE$ can be expanded to first order:

$$\hat{G}(E + dE) \approx \hat{G}(E) + \frac{d\hat{G}(E)}{dE}dE \tag{A.1}$$

Multiplying both sides of equation (A1) by $\hat{G}^*(E)$ gives

$$\hat{G}^*(E)\hat{G}(E + dE) \approx \hat{G}^*(E)\hat{G}(E) + \hat{G}^*(E)\frac{d\hat{G}(E)}{dE}dE = 1 + i\hat{G}^*(E)\frac{d\hat{G}(E)}{dE}dE$$

Taking the trace of both sides of the previous relation results in

$$Tr(\hat{G}^*(E)\hat{G}(E + dE)) = 1 + Tr\left(\hat{G}^*(E)\frac{d\hat{G}(E)}{dE}\right)dE + \ldots \tag{A.2}$$

Introducing the geometric phase, $\eta(E)$, the normalized Green’s function can be now written as $\hat{G}(E + dE) = e^{i\eta(E+dE)} \sim e^{i\left(\eta(E)+\frac{d\eta(E)}{dE}dE\right)} = e^{i\eta(E)}e^{i\frac{d\eta(E)}{dE}dE}$.

Since $\hat{G}^*(E) \propto e^{-i\eta(E)}$, we can rewrite Eq. (A.2) as

$$e^{i\frac{d\eta(E)}{dE}dE} \sim 1 + i\frac{d\eta(E)}{dE}dE = 1 + iBC(E)dE \tag{A.3}$$

Using the definition of Eq. (2), comparison of the two imaginary terms in Eq. (A.3) leads to

$$\frac{d\eta(E)}{dE} = BC(E) \tag{A.4}$$

From the definition of $\eta(E)$, one notes that $BC(E)$ must be real. It is informative to obtain the relation given by Eq. (A.4) by directly calculating $BC(E)$ using Eq. (1) in the main text:

$$BC(E) = -iTr\left(\hat{G}^*(E)\frac{d\hat{G}(E)}{dE}\right) = -iTr\left\{\frac{G^*}{G^*G}\frac{dG}{dE} - \frac{1}{2G^*G}\frac{d(G^*G)}{dE}\right\} \tag{A.5}$$

By ensuring that $BC(E)$ is real, it is easy to show

$$BC(E) = Im\ Tr\left(\frac{1}{G}\frac{dG}{dE}\right) = Im\ Tr\left(\frac{dlnG}{dE}\right) \tag{A.6}$$

or

$$BC(E) = Im\left(\frac{d}{dE}(TrlnG)\right) = -Im(TrG) \tag{A.7}$$

To derive Eqs. (A.6) and (A.7), we have used well-established Green's functions identities related to the properties of the Green's function in the space of its Eigen values (Deymier and Runge, 2017).

Appendix B

The calculation of the Green's function of a system composed of semi-infinite simple cubic crystal, cleaved along the (001) face (i.e. ground) and a finite 1-D mass-spring chain coupled to a ground surface site via a spring with constant, β_I, (tree-ground anchor) begins with the block matrix describing the Green's function of the uncoupled system ($\beta_I = 0$):

$$\vec{\vec{G}}_S = \begin{pmatrix} \vec{\vec{g}}_{S1} & \vec{0} \\ \vec{0} & \vec{\vec{g}}_{S2} \end{pmatrix}, \tag{B.1}$$

where $\vec{\vec{g}}_{S1}$ is the Green's function of the semi-infinite discrete lattice and where $\vec{\vec{g}}_{S2}$ is the Green's function of the mass-spring chain. $\vec{\vec{g}}_{S1}$, therefore, describes elastic waves with any polarization in the three-dimensional semi-infinite space of the cleaved lattice. For the sake of simplicity, we are choosing the masses and spring constants of the cubic lattice and chain to be identical, m and β. The spacing between masses along the chain is a. The Green's function of a finite harmonic chain of length L (for n, $n'\varepsilon[1, L]$), with coordinates along the chain expressed as integer multiples of that spacing: $x = na$, (Deymier, 2013) is given by

$$g_{S2}(n, n') = \frac{m'}{\beta'}\left[\frac{t^{|n-n'|+1} + t^{n+n'}}{t^2-1} + \frac{t^{2L+1}}{(t^2-1)(1-t^{2L})}(t^{n'-n} + t^{n-n'} + t^{1-n-n'} + t^{n+n'-1})\right] \tag{B.2}$$

where

$$t = \begin{cases} \xi - (\xi^2-1)^{1/2}\ if\ \xi > 1 \\ \xi + (\xi^2-1)^{1/2}\ if\ \xi < -1 \\ \xi + i(1-\xi^2)^{1/2}\ if\ -1 \le \xi \le 1 \end{cases} \tag{B.3}$$

with

$$\xi = 1 - \frac{m\omega^2}{2\beta} \tag{B.4}$$

The frequency $\omega \in [0, \omega_0]$ with $\omega_0 = 2\sqrt{\frac{\beta}{m}}$. A tree is modeled as a mass-spring chain with $L = 4$.

The Green's function of the semi-infinite cubic lattice possesses translational periodicity in the plane of the (001) surface and is written as a two-dimensional Fourier transform:

$$\vec{\vec{g}}_{S1}(\omega, x_1, x_2, x_3) = \frac{1}{(2\pi)^2}\int_{-\frac{\pi}{a}}^{\frac{\pi}{a}} dk_1 \int_{-\frac{\pi}{a}}^{\frac{\pi}{a}} dk_2\, e^{i(k_1x_1+k_2x_2)}\vec{\vec{g}}_{S1}(\omega, k_1, k_2, x_3) \tag{B.5}$$

Here, (x_1, x_2) is a site on the (001) surface of the semi-infinite lattice. The surface is located at $x_3 = 0$. The lattice parameter of the simple cubic lattice is also taken as a. The Fourier transform of the Green's function $\vec{\vec{g}}_{S1}$ is given by (Akjouj et al., 1993)

$$\vec{\vec{g}}_{S1}(\omega, k_1, k_2, x_3) = \frac{m}{\beta}\frac{t^{|n_3-n_3'|+1} + t^{2-(n_3+n_3')}}{t^2-1} \tag{B.6}$$

with $n_3^{(')} = \frac{x_3^{(')}}{a}$.

We note that $g_{S1}(\omega, x_1, x_2, x_3 = 0)$ is calculated as the two-dimensional Fourier transform (Eq. (B.5) of Eq. (B.6)). Eq. (B.6) requires the calculation of t using Eq. (B.3). For the Fourier transform, we use the dispersion relation for a simple cubic harmonic lattice: $\omega^2 = \frac{2\beta}{m}(3 - \cos k_1a - \cos k_2a - \cos k_2a)$ to define

$$\xi = 3 - \cos k_1a - \cos k_2a - \frac{m\omega^2}{2\beta} \tag{B.7}$$

If we define a position on the surface of the cubic lattice: $p_i = (x_1^{(i)}, x_2^{(i)}, 0)$, then we only calculate for every frequency $\omega \le \omega_0$: $g_{S1}(p_ip_j) = g_{S1}(p_i - p_j = (x_1^{(j)} - x_1^{(i)}, x_2^{(j)} - x_2^{(i)}, 0))$ for $(x_1^{(j)} - x_1^{(i)}, x_2^{(j)} - x_2^{(i)}, 0) = \{(0,0,0),\ (0,1a,0),\ (0,2a,0),\ (1a,0,0),\ (2a,0,0),\ (1a,1a,0),\ (1a,2a,0),\ (2a,1a,0)\}$. All other g_{S1} are neglected in this paper. Hence, we consider a cut off of $|p_i - p_j| = \sqrt{5}a$ for the Green's function $g_{S1}(p_ip_j)$. We denote by $g_{S1}(|p_i - p_j| = 0) = g_{00}$, $g_{S1}(|p_i - p_j| = 1a) = g_{01}$, $g_{S1}(|p_i - p_j| = 2a) = g_{02}$, $g_{S1}(|p_i - p_j| = \sqrt{2}a) = g_{11}$, and $g_{S1}(|p_i - p_j| = \sqrt{5}a) = g_{12}$. The numerical functions $g_{S1}(p_ip_j, \omega)$ are replaced by fits to functions of frequency, ω. These fits are given in Deymier and Runge (2018).

Following the IRT, we define a coupling operator that enables us to couple a site 1 of a mass-spring chain (base of a tree) to a site X (effectively $X=(x_1, x_2, x_3 = 0)$) on the surface of the cubic lattice (i.e. ground):

$$\vec{\vec{V}}_I = \begin{pmatrix} V_I(X,X) & V_I(X,1) \\ V_I(1,X) & V_I(1,1) \end{pmatrix} = \begin{pmatrix} \frac{-\beta_I}{m} & \frac{\beta_I}{m} \\ \frac{\beta_I}{m} & \frac{-\beta_I}{m} \end{pmatrix}. \tag{B.8}$$

For the sake of simplicity, we will take $\beta_I = \beta$. IRT introduces the surface operator expressed in the space M of coupled interface sites:

$$\vec{A}_0(MM) = \begin{pmatrix} A(X,X) \\ A(X,1) \\ A(1,X) \\ A(1,1) \end{pmatrix} = \begin{pmatrix} V_I(X,X)g_{S1}(X,X) \\ V_I(X,1)g_{S2}(1,1) \\ V_I(1,X)g_{S1}(1,X) \\ V_I(1,1)g_{S2}(1,1) \end{pmatrix}. \tag{B.9}$$

The diffusion matrix takes then the form of a 2 × 2 matrix in the space of the interface sites, *M*:

$$\vec{\vec{\Delta}}(MM) = \begin{pmatrix} 1 + A(X,X) & A(X,1) \\ A(1,X) & 1 + A(1,1) \end{pmatrix} = \begin{pmatrix} 1 + V_I(X,X)g_{S1}(X,X) & V_I(X,1)g_{S2}(1,1) \\ V_I(1,X)g_{S1}(1,X) & 1 + V_I(1,1)g_{S2}(1,1) \end{pmatrix} \tag{B.10}$$

The phase difference (normalized to π) of elastic modes in the space M between the coupled system (trees elastically anchored to the ground) and the uncoupled system (trees not anchored) is then obtained from the relation

$$\eta(\omega) = -\frac{1}{\pi} Im\left[\ln(det\vec{\vec{\Delta}}(MM))\right] \tag{B.11}$$

This is effectively the phase accumulated by the wave scattered by the elastically anchored mass-spring chains. The variation in density of states due to the coupling is then obtained from the relation

$$\Delta n(\omega) = \frac{d\eta(\omega)}{d(\omega^2)} \tag{B.12}$$

Δn is the variation of the vibrational density of states between the trees anchored to the ground system and the reference system (i.e., cubic lattice with uncoupled trees).

In the following we generalize the application of the IRT to multiple trees (mass spring chains) anchored on the surface of the ground cubic lattice. For this we consider N_c identical mass-spring chains anchored at multiple sites on the (001) surface of the simple cubic lattice. The space *M* for the system is now defined as

$$M = \{p_1 = (0,0,0), 1, p_2 = (x'_1, x'_2, 0), 1', p_3 = (x''_1, x''_2, 0), 1'', ..., p_{N_c} = (x_1^{(N_c-1)}, x_2^{(N_c-1)}, 0), 1^{(N_c-1)}\} \tag{B.13}$$

We have located the first finite mass-spring chain at the origin on the lattice surface. In this case, the coupling operator is a $2N_c \times 2N_c$ matrix of the form

$$\vec{\vec{V}}_I = \frac{\beta_I}{m}\begin{pmatrix} -1 & 1 & 0 & 0 & ... & 0 & 0 \\ 1 & -1 & 0 & 0 & ... & 0 & 0 \\ 0 & 0 & -1 & 1 & ... & 0 & 0 \\ 0 & 0 & 1 & -1 & ... & 0 & 0 \\ \vdots & \vdots & \vdots & \vdots & ... & \vdots & \vdots \\ 0 & 0 & 0 & 0 & 0 & -1 & 1 \\ 0 & 0 & 0 & 0 & 0 & 1 & -1 \end{pmatrix}. \tag{B.14}$$

To calculate $\vec{\vec{\Delta}}(MM) = \vec{\vec{I}}(MM) + \vec{\vec{V}}_I(MM)\vec{\vec{G}}_S(MM)$, one needs the Green's function of the unanchored system, $\vec{\vec{G}}_S(MM)$, which takes the form

$$\vec{\vec{G}}_s(MM) = \begin{pmatrix} g_{S1}(p_1p_1) & 0 & g_{S1}(p_1p_2) & 0 & g_{S1}(p_1p_3) & 0 & ... & g_{S1}(p_1p_{N_c}) & 0 \\ 0 & g_{S2}(11) & 0 & 0 & 0 & 0 & ... & 0 & 0 \\ g_{S1}(p_2p_1) & 0 & g_{S1}(p_2p_2) & 0 & g_{S1}(p_2p_3) & 0 & ... & g_{S1}(p_2p_{N_c}) & 0 \\ 0 & 0 & 0 & g_{S2}(1'1') & 0 & 0 & ... & 0 & 0 \\ g_{S1}(p_3p_1) & 0 & g_{S1}(p_3p_2) & 0 & g_{S1}(p_3p_3) & 0 & ... & g_{S1}(p_3p_{N_c}) & 0 \\ 0 & 0 & 0 & 0 & 0 & g_{S2}(1^{(2)}1^{(2)}) & ... & 0 & 0 \\ \vdots & \vdots & \vdots & \vdots & \vdots & \vdots & \vdots & \vdots & \vdots \\ g_{S1}(p_{N_c}p_1) & 0 & g_{S1}(p_{N_c}p_2) & 0 & g_{S1}(p_{N_c}p_3) & 0 & ... & g_{S1}(p_{N_c}p_{N_c}) & 0 \\ 0 & 0 & 0 & 0 & 0 & 0 & ... & 0 & g_{S2}(1^{(N_c-1)}1^{(N_c-1)}) \end{pmatrix} \tag{B.15}$$

In this matrix, the odd entries (rows or columns) correspond to locations on the surface of the ground lattice and the even entries correspond to the position of the first mass the finite mass-spring chains.

The diffusion matrix in the space *M* is

$$\vec{\vec{\Delta}}(MM) = \vec{\vec{I}} + \vec{\vec{A}}(M,M) = \vec{\vec{I}} + \vec{\vec{V}}_I\vec{\vec{G}}_s(MM). \tag{B.16}$$

The phase difference is again given by Eq. (B.11).

References

Akjouj, A., Sylla, B., Dobrzynski, L., 1993. Introduction to a theory of composite systems – simple examples of lamellar materials. Ann. Readapt. Med. Phys. 18, 363.

Berry, M.V., 1984. Quantal phase factors accompanying adiabatic changes. Proceedings of the Royal Society A 392, 45.

Campillo, M., 2006. Phase and correlation in 'Random' seismic fields and the reconstruction of the green function. Pure appl. geophys. 163, 475.

Carrer, M., Castagneri, D., Popa, I., Pividori, M., Lingua, E., 2018. Tree spatial patterns and stand attributes in temperate forests: the importance of plot size, sampling design, and null model. For. Ecol. Manage. 407, 125.

Colombi, A., Roux, P., Guenneau, S., Guéguen, P., Craster, R.V., 2016. Forests as a natural seismic metamaterial: rayleigh wave bandgaps induced by local resonances. Sci. Rep. 6, 19238.

Derode, A., Larose, E., Campollo, M., Fink, M., 2003. How to estimate the Green's function of a heterogeneous medium between two passive sensors? Application to acoustic waves. Appl. Phys. Lett. 83, 3054.

Acoustic metamaterials and phononic crystals. In: In: Deymier, P.A. (Ed.), Springer Series in Solid State Sciences Vol. 173 Springer, Berlin.

Deymier, P.A., Runge, K., 2017. Sound topology, duality, coherence and wave-mixing: an introduction to the emerging new science of sound. Springer Series in Solid-State Sciences Vol. 188.

Deymier, P.A., Runge, K., 2018. Phase properties of elastic waves in systems constituted of adsorbed diatomic molecules on the (001) surface of a simple cubic crystal. J. of Applied Physics 123, 125106.

Díaz-Delgado, R., Lucas, R., Hurford, C. (Eds.), 2017. The Roles of Remote Sensing in Nature Conservation. Springer International Publishing.

Dobrzynski, L., 1987. Interface response theory of discrete superlattices. Prog. Surf. Sci. 26, 103.

Dobrzynski, L., 1988. Interface response theory of composite systems. Surf. Sci. 200, 435.

Franklin, J., 2010. Mapping Species Distributions: Spatial Inference and Prediction. Cambridge University Press.

Greig-Smith, P., 1952. The use of random and contiguous quadrats in the study of the structure of plant communities. Ann. Bot. 16, 293.

Greig-Smith, P., 1983. Quantitative Plant Ecology. University of California Press.

Larson, A.J., Churchill, D., 2012. Tree spatial patterns in fire-frequent forests of western North America, including mechanisms of pattern formation and implications for designing fuel reduction and restoration treatments. For. Ecol. Manage. 267, 74.

Maurel, A., Marigo, J.-J., Pham, K., Guenneau, S., 2018. Conversion of Love waves in a forest of trees. Phys. Rev. B 98, 134311.

Mullet, T.C., Gage, S.H., Morton, J.M., Huettmann, F., 2016. Temporal and spatial variation of a winter soundscape in south-central Alaska. Landscape Ecol. 31 (1117).

Ohse, B., Huettmann, F., Ickert-Bond, S., Juday, G., 2009. Modeling the distribution of white spruce (*Picea glauca*) for Alaska with high accuracy: an open access role-model for predicting tree species in last remaining wilderness areas. Polar Biol. 32 (1717).

Sahin, Y.G., Ince, T., 2009. Early forest fire detection using radio-acoustic sounding system. Sensors 9 (1485).

Sanchez-Sesma, F.J., Campillo, M., 2006. Retrieval of the green's function from cross correlation: the canonical elastic problem. Bull. Seismol. Soc. Am. 96 (1182).

Sharma, G., 2018. Acoustic signal classification for deforestation monitoring: tree cutting problem. J. Comput. Sci. Syst. Biol. 11, 178.

Stein, S., Wysession, M., 2009. An Introduction to Seismology, Earthquakes, and Earth Structure. John Wiley & Sons.

Turner, A., Fischer, M., Tzanopoulos, J., 2018. Sound-mapping a coniferous forest—-perspectives for biodiversity monitoring and noise mitigation. PlosOne 13, e0189843.

Young, B.D., Yarie, J., Verbyla, D., Huettmann, F., Stuart Chapin III, F., 2018. Mapping aboveground biomass of trees using forest inventory data and public environmental variables within the Alaskan boreal Forest. In: Humphries, G., Magness, D.R., Huettmann, F. (Eds.), Machine Learning for Ecology and Sustainable Natural Resource Management, pp. 141–160.

Zhang, X., Xiao, M., Cheng, Y., Lu, M.-H., Christensen, J., 2018. Topological sound. Nat. Commun. Phys. 1, 97.